ENERGY MINIMIZATION APPROACH FOR ONLINE DATA ASSOCIATION WITH MISSING DATA

Abir El Abed, Séverine Dubuisson and Dominique Béréziat
Laboratoire d'Informatique de Paris 6, Université Pierre et Marie Curie
104 avenue du Président Kennedy, 75016 Paris, France

Keywords: Online data association, energy minimization, prior informationless and non-rigid motion.

Abstract: Data association problem is of crucial importance to improve online target tracking performance in many difficult visual environments. Usually, association effectiveness is based on prior information and observation category. However, some problems can arise when targets are quite similar. Therefore, neither the color nor the shape could be helpful informations to achieve the task of data association. Likewise, problems can also arise when tracking deformable targets, under the constraint of missing data, with complex motions. Such restriction, *i.e.* the lack in prior information, limit the association performance. To remedy, we propose a novel method for data association, inspired from the evolution of the target dynamic model, and based on a global minimization of an energy vector. The main idea is to measure the absolute geometric accuracy between features. Its parameterless constitutes the main advantage of our energy minimization approach. Only one information, the position, is used as input to our algorithm. We have tested our approach on several sequences to show its effectiveness.

1 INTRODUCTION

Traditionally, multiple object tracking deals with the state estimation of moving targets. A track is a state trajectory estimated from the available measurements that have been associated with the same target (Vermaak et al., 2005). The main difficulty comes from the assignment of a given measurement to a target model. These assignments are generally unknown, as are the true target models. The idea of data association remains to find a partition of observations such that each element is generated by a target, or clutter, whose statistical properties differ from one target to another. The literature contains some classical approaches: we can distinguish the deterministic approaches from the probabilistic ones.

Deterministic approaches select the best of several candidate associations, without taking into account its context correctness, by using a score function (Vermaak et al., 2005). The simplest deterministic method for data association is the Nearest-Neighbor Standard Filter (NNSF) (Rong and Bar-Shalom, 1996) that selects the closest validate measurement to a predicted target and uses it for its state estimation. Usually, the distance measure used is the Mahalanobis one. Since the filter does not take into account the possibility of incorrect associations, the performance of this filter might be poor in some cases, resulting in an incorrect association between measurements and targets. In some tracking applications, the color is also exploited for the problem of data association. One can measure the color histogram difference between a measurement and the objects of the previous frame using the histogram intersection technique. Unfortunately, the color metric is not sufficient for a correct data association in many cases: for deformable objects, which color distribution may differ from one frame to another, or in case of several quite identical objects.

Probabilistic approaches are based on posterior probability and make an association decision using the probability error (Rasmussen and Hager, 2001). Among probabilistic approaches, we can cite the most general one, called Multiple Hypothesis Tracking (MHT) (Vermaak et al., 2005). In MHT, the multiple hypotheses are formed and propagated, implying the

El Abed A., Dubuisson S. and Béréziat D. (2007).
ENERGY MINIMIZATION APPROACH FOR ONLINE DATA ASSOCIATION WITH MISSING DATA.
In *Proceedings of the Second International Conference on Computer Vision Theory and Applications - IU/MTSV*, pages 371-378

calculation of every possible hypothesis. Due to the exploring of a high-dimensional joint state space, this method is computational intensive. Another strategy for multiple target tracking association is the Probability Data Association Filter (PDAF) (Rasmussen and Hager, 2001), that assigns an association probability to each measurement and uses these probabilities to weight the measurements for track update. The original PDAF formulation has some limitations: it assumes that all measurements come from the track being updated, that is not true in case of dense target conditions. The Joint Probability Data Association (JPDA) (Fortmann et al., 1983) uses a weighted sum of all measurements near the predicted state, each weight corresponding to the posterior probability for a measurement to come from a target. JPDAF provides an optimal data solution in the Bayesian framework. However, the number of possible hypothesis increases rapidly with the number of targets, requiring prohibitive amount of time calculating.

Generally, an effective data association method is based on prior information and observation category. If we have a lack of prior information, that can happen when the observer has no information concerning the system, the association task becomes difficult. Such cases can occur when the observed system is deformable, moreover, when we observe, with minor information about the movement, multiple objects that are quite similar even non distinguishable. It can be more complicated if we have a considerable interval of time between observations and if the observer has no prior information about object's motion. Likewise, if we only observe target positions, we can face a measurement that is equidistant from several targets: all target association probabilities are relatively the same and it is difficult to associate the good measurement with the good target. As far as, no association method can handle all the cases illustrated previously.

In this paper, we propose a novel method for data association based on the minimization of an energy magnitude $\|\vec{E}\|$ and adapted to the circumstances described previously. This energy, inspired from target motion, measures the geometric accuracy between features and associates the measurement y (given by sensor) with the target k if $\|(\vec{E}_k)_y\|$ is minimized. The main advantages of this energy are followed. It does not require parameters or prior knowledge and is not a time-consumer. Exclusively one information about targets is used: positions. Besides, it can handle the problem of association when a measurement falls within the validation region for several targets and is equidistant from them.

The outline of this paper is as follows. In Section 2, we expose our energy minimization approach, derive its geometrical representation and its mathematical model. The proposed method is then evaluated and tested on several sequences in Section 3. Finally, concluding remarks and perspective are given in Section 4.

2 ENERGY MINIMIZATION APPROACH FOR DATA ASSOCIATION

We first need to define some terms that will be often used in this paper. We dispose a video sequence describing a dynamical scene. It is observed by a set of sensors. Each observation contains at least one measurement: a position. The number of available measurements can differ from one observation to another. Each measurement can be associated with a specific object in the scene (*i.e.* target), or can be a false alarm. At a specific time t, observations are assumed to be available from N_{obs} sensors. The set of observations coming from all sensors is given by $y = (y^1, ..., y^{N_{\text{obs}}})$, where $y^i = (y^i_1, ..., y^i_{M^i})$ is the vector containing the M^i measurements coming from the i^{th} sensor, also called observation. We suppose that each sensor can generate at most one observation, containing at least one measurement at a particular time step and that the number of measurements delivered by the sensors varies with time. When an observation is available, our goal is to associate a maximum one measurement per target. The total number of targets is K.

2.1 Energy Minimization Modelling

Generally, an effective data association method is based on measurement category. When the measurement is limited to a position, and falls inside the validation region of several targets and is equidistant from them (see Figure 1.a), it will be associated with all these targets if we use the NNSF or Monte Carlo JPDAF approaches. As well as, in multiple target tracking, feature targets can be quite similar. Accordingly, even if information about their color distribution or shape is available, the association task is difficult under such assumptions or impossible in case of complex dynamics.

In this paper, we propose an algorithm for data association restricted to one category of measurement: the position. Furthermore, we affirm the total lack of prior information concerning targets: exclusively the two anterior predicted positions are used. We will first give the concept of our approach before starting its

mathematical modeling. Our intention is to formalize a method able to associate a measurement according to the restrictions displayed in Section 1. We define a novel energy vector $\vec{E}$ in the direct affine euclidean space $(O,\vec{i},\vec{j},\vec{k})$. This energy is inspired from the target's dynamic evolution. The dynamic model is described in terms of displacements in the target space (x,y). If we only consider the linear translation in one direction, the problem of data association is limited to the computation of the Mahalanobis distance energy $\vec{E}^1$ (see after for details). Thus, in case of complex dynamics such as non linear displacements, oscillatory motions and non-constant velocities, we are vis-a-vis a problem because $\vec{E}^1$ will be an insufficient informative source. To remedy, we incorporate a second energy term $\vec{E}^2$ which measures the absolute accuracy between the dynamic features and indicates how much their parameters are close. Moreover, we distinguish some dynamic cases, that will be clarified by geometric descriptions afterward, for whose we need to compensate $\vec{E}^2$ by the proximity energy evolution $\vec{E}^3$ for a better association of te available data.

The energy vector $\vec{E}$ is only computed when the measurement falls within several validation regions. We consider a measurement as a clutter if it is not included in any validation region. In our case, the validation region is an ellipsoid that contains a given probability mass under the Gaussian assumption. The minor and major axes of this ellipsoid are respectively given by the largest and smallest eigenvalues of the covariance matrix, their directions are given by the corresponding eigenvectors, and the center is the mean of the target.

We define the energy vector between the k^{th} target $(k = 1,\ldots,K)$ and the measurement y^i_j, *i.e.* j^{th} measurement of the i^{th} sensor, by:

$$(\vec{E}_k)_{y^i_j} = \frac{1}{\sqrt{3}} \sum_{l=1}^{3} \alpha_l (\vec{E}^l_k)_{y^i_j} \qquad (1)$$

where $\alpha_l = \frac{1}{\sum_{k=1}^{K} ||(\vec{E}^l_k)_{y^i_j}||}$ is a weighted factor introduced to sensibly emphasize the relative importance attached to the energy quantities $\vec{E}^l$.

Before interpreting each energy, we consider a target A and a measurement y^i_j. Besides, we call (see Figure 1 for illustration):

- $\hat{A}(t-2)$, $\hat{A}(t-1)$, $\hat{A}(t)$ and $\hat{A}_1(t+1)$: prediction of A at $t-2$, $t-1$, t and $t+1$ by using the initial dynamic model;
- $\hat{A}_2(t+1)$: prediction of A at $t+1$ by using the updated dynamic model. In this case, the measurement y^i_j is associated with the target A at instant t and the parameters of the dynamic model are updated according to y^i_j.

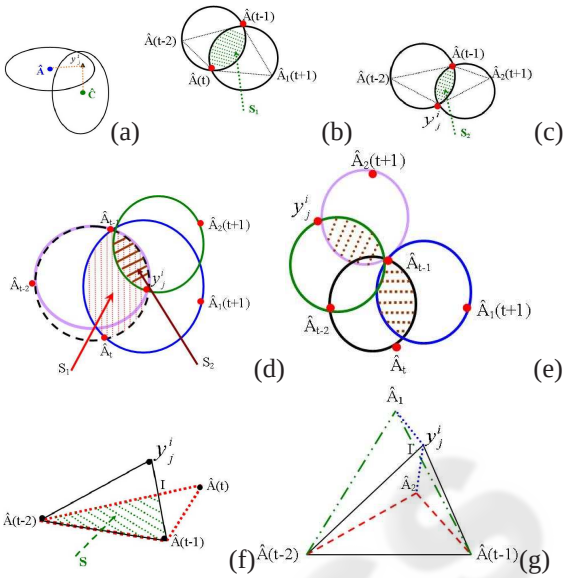

Figure 1: (a) Measurement y^i_j falls inside the two validation regions of A and C; (b-c-f) Intersection surfaces $\{S_1,S_2,S\}$; (d-e) Difference between the sufaces S_1 and S_2 extracted from two dynamical models; (g) Intersection surfaces where two predictions at instant t, $\hat{A}_1$ and $\hat{A}_2$, are equidistant from y^i_j.

Prediction is based on the use of a dynamic model which parameters are generally fixed by learning from a training sequence to represent plausible motions such as constant velocities or critically damped oscillations (North et al., 2000; Blake and Isard, 1998). For complex dynamics, such as non-constant velocities or non-periodic oscillations, the choice of the parameters for an estimation algorithm is difficult. Furthermore, the learning step becomes particularly more difficult in the case of missing data, because the dynamic between two successive observations is unknown. For these reasons, the parameters of our dynamic model are set in an adaptive and automated way once a measurement is available (Abed et al., 2006).

The energy vector $(\vec{E}_k)_{y^i_j}$ contains three components, $\{\vec{E}^1,\vec{E}^2,\vec{E}^3\}$, as defined below:

1. The Mahalanobis distance energy, $(\vec{E}^1_k)_{y^i_j}$, measures the distance between a measurement y^i_j occurred at instant t and the prediction of the target A at $t-1$. This energy is sufficient to associate the available measurement if the target's motion is limited to translations in one direction (case of linear displacements). It is given by:

$$\begin{aligned}(\vec{E}^1_k)_{y^i_j} &= \|(\vec{E}^1_k)_{y^i_j}\|\vec{i} \qquad (2)\\ &= \sqrt{(y^i_j-\hat{A}(t-1))^T \hat{\Sigma}_k^{-1} (y^i_j-\hat{A}(t-1))}\,\vec{i}\end{aligned}$$

where Σ_k is the covariance matrix of the k^{th} target (we designe the k^{th} target by A in the equation).

2. To consider the case of complex dynamics, such as oscillatory motions or non-constant velocities, we have added the absolute accuracy evolution energy $(\vec{E}_k^2)_{y_j^i}$. It introduces the notion of the geometric accuracy between two sets of features whose dynamic evolution is different. The description of both models are followed:
   - The updated dynamic model set considers that the available measurement y_j^i at t is generated by the k^{th} target and updates the parameters of its dynamic model to predict the new state of the target k at $t+1$;
   - The not updated dynamic model set predicts the new state at $t+1$ without considering the presence of the measurement, *i.e.* without updating the parameters of the dynamic model.

   $(\vec{E}_k^2)_{y_j^i}$ extends a numerical estimation of the closeness between two dynamic models. Our idea aims to evaluate the parameters of the dynamic model in two cases if the measurement y_j^i arises from this target or no. We first predict the states $\hat{A}_1(t+1)$ and $\hat{A}_2(t+1)$ of the target at $t+1$. We then determine S_1, the intersection surface between the two circumscribed circles of the triangles $(\hat{A}(t-2),\hat{A}(t-1),\hat{A}(t))$ and $(\hat{A}(t-1),\hat{A}(t),\hat{A}_1(t+1))$, and S_2, the intersection surface between the two circumscribed circles of the triangles $(\hat{A}(t-2),\hat{A}(t-1),y_j^i)$ and $(\hat{A}(t-1),y_j^i,\hat{A}_2(t+1))$, (see Figures(1.b-c)). $(\vec{E}_k^2)_{y_j^i}$ is minimized when the similarity between both dynamic models is maximized and is given by:

$$(\vec{E}_k^2)_{y_j^i} = \|(\vec{E}_k^2)_{y_j^i}\|\vec{j} = |S_1 - S_2|\vec{j} \qquad (3)$$

   We compare these two sets to measure the ratio of similarity, defined by $R_s = 1 - \|(\vec{E}_k^2)_{y_j^i}\|$, between the predictions at $t+1$ given by two different dynamic models for target k. Increasing this ratio maximizes the probability that the measurement y_j^i is generated by target k and the resemblance between two dynamic models.
   A question might be asked: is the component $\vec{E}^2$ able to handle all type of motions ?
   Indeed, $\vec{E}^2$ evaluates a numerical measure of similarity between dynamic models. This measurement depends on the difference between two surfaces. It is considered as reliable if both positions, $\hat{A}(t)$ and y_j^i, are on the same side comparing to axis $(\hat{A}_{t-2}\hat{A}_{t-1})$, see Figure 1.d. In Figure 1.e, we show the case where both surfaces, S_1 and S_2, are quite similar, which imply $\vec{E}^2$ to be null. This case can occur when the positions of $\hat{A}(t)$ and y_j^i are diametrically opposite or when their positions are in different side comparing to axis $(\hat{A}_{t-2}\hat{A}_{t-1})$. In such cases, the energy $\vec{E}^2$ is not a sufficient informative source to achieve the task of association. To compensate this energy, we then incorporate the third energy $\vec{E}^3$.

3. The proximity energy evolution, $(\vec{E}_k^3)_{y_j^i}$, is the inverse of the surface S defined by the common area between the two triangles $(\hat{A}(t-2),\hat{A}(t-1),y_j^i)$ and $(\hat{A}(t-2),\hat{A}(t-1),\hat{A}(t))$ (see the dotted area of Figure 1.f). This energy evaluates the absolute accuracy between the prediction $\hat{A}(t)$ and the measurement y_j^i at instant t. Increasing S means that the prediction and measurement at instant t are close. This energy is given by:

$$(\vec{E}_k^3)_{y_j^i} = \|(\vec{E}_k^3)_{y_j^i}\|\vec{k} = \frac{1}{S}\vec{k} \qquad (4)$$

   Another question could be asked: why do we have to use the intersection surface instead of only calculating the distance between the measurement y_j^i and the prediction of target's position at instant t? In Figure 1.g, we have two predictions at instant t, $\hat{A}_1$ and $\hat{A}_2$. They are both equidistant from the measurement y_j^i. If we only compute the distance to measure the proximity energy, we will get that both models have the same degree of similarity with the initiation model defined by the dynamic model of points $(\hat{A}(t-2),\hat{A}(t-1),y_j^i)$. This result leads to a contradiction with the reality. This problem can be explained by the fact that if they have both the same degree of similarity with the third dynamic model, we can conclude that their corresponding targets have the same dynamic. For this reason, we have chosen to evaluate the similarity by extracting the intersection surface between triangles. We can remark in Figure 1.g that these intersection surfaces are very different, which leads to a different measure in the degree of similarity.

Finally, the measurement y_j^i is associated with the target k if its energy magnitude is minimized:

$$\begin{aligned} \gamma_{y_j^i \to k} &= \left\{ \min_{k=1,\ldots,K} (\|(\vec{E}_k)_{y_j^i}\|) \right\} \qquad (5) \\ &= \left\{ \min_{k=1,\ldots,K} \left(\frac{1}{\sqrt{3}} \sqrt{\sum_{l=1}^{3} \alpha_l^2 \|(\vec{E}_k^l)_{y_j^i}\|^2)} \right) \right\} \end{aligned}$$

   with $0 \leq \alpha_l \leq 1$ and $0 \leq \|(\vec{E}_k)_{y_j^i}\| \leq 1$.

We have described a novel approach for data association based on the minimization of an energy magnitude whose components are extracted from geometrical representations (area and distance) constructed

with measurements, previous states and predictions. The purpose of choosing a geometrical definition for these energies refers to:

- show the geometrical continuity of the system between predictions and previous states using two different dynamic models;
- measure the similarity between predictions, at a particular time for the same object, using two different dynamic models, that logically must be quite similar because they represent the same system.

3 EXPERIMENTAL RESULTS

3.1 Synthetic Test

To expose the performance of our energy minimization approach, we suggest the synthetic example of Figure 2, which explores the case of an oscillatory motion with a constant phase. It shows two targets T_1 and T_2 whose dynamic models are defined by two different sinusoids, $\sin(x)$ and $\sin(2x)+0.5$. The measurement y (full square in Figure 2), is equidistant from both targets and falls in their validation regions. In such case, both targets are candidates to be associated with this measurement. We compute the energy magnitude for each target (see Table 1) and obtain that $\|(\vec{E}_1)_y\| < \|(\vec{E}_2)_y\|$ and the measurement is associated with T_1.

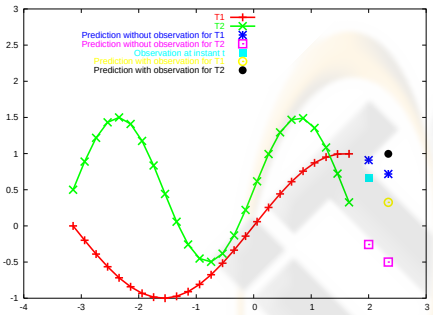

Figure 2: Sinusoids with a constant phase: the dotted lines represent the trajectories of targets T_1 and T_2. The full square is the measurement y. The dotted squares and blue stars are the predictions of T_2 and T_1 at instants $\{t+1, t+2\}$ without taking into account the presence of the observation. The dotted and full circles are the predictions of T_1 and T_2 if we consider that the observation is associated with both targets.

We give another example where the motion of both targets is given by a sinusoid with a non periodic phase, see Figure 3. At instant $t-1$, both targets have the same position as shown in Figure 3. If we use the NNSF method, the measurement will be associated with both targets since it is equidistant from

Table 1: Energy magnitude computation for targets T_1 and T_2.

k	$\alpha_i\|(\vec{E}_k^i)_y\|$			$\|(\vec{E}_k)_y\|$
1	0.5	0.0001	0.4821	0.5278
2	0.5	0.9999	0.5179	0.9362

them. To improve the association result, we compute the energy magnitude for each target and the results are given in Table 2. We obtain $\|(\vec{E}_1)_y\| < \|(\vec{E}_2)_y\|$ and the measurement is associated with T_1.

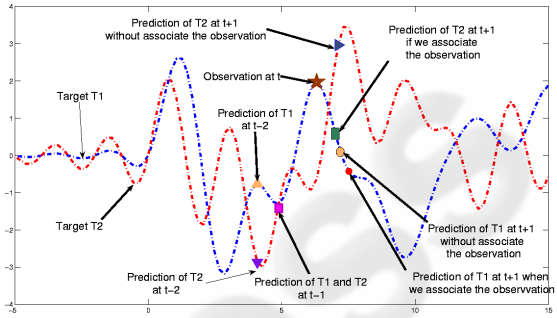

Figure 3: Sinusoids with non-constant phases: the dotted lines represent the trajectories of targets; the shapes (squares, circles, triangles) are their predictions at different instants.

Table 2: Energy magnitude computation for T_1 and T_2.

k	$\alpha_i\|(\vec{E}_k^i)_y\|$			$\|(\vec{E}_k)_y\|$
1	0.5	0.0970	0.3094	0.3441
2	0.5	0.9030	0.6906	0.7170

3.2 Van-Plane Test

In the following experiment, the available observation at instant t contains two measurements M_1 and M_2, each one represents a position in the target space (x,y). The first row in Figure 4 contains the frames at $\{t-2, t-1, t\}$ where two targets $\{T_1, T_2\}$, the van and the plane, are present. If we look at the position of these measurements on the real frame at t (right image in Figure 4), we observe that M_1 is closed to T_1 and M_2 to T_2. In the second and third rows, we show the predictions of both targets by evaluating two different dynamic models in the target space (x,y). We point out that the horizontal and the vertical axis of the frame are represented by the y-axis and x-axis in the target space. We can remark that the distance from T_1 to M_1 is larger than the one from T_1 to M_2, see the Mahalanobis distance energy $\alpha_1\|(\vec{E}_1^1)_{\{M_1,M_2\}}\|$ in Table 3. Hence, if we use the Nearest Neighbor association method, the target T_1 will be associated to

M_2 which causes a contradiction with the reality. To remedy, we compute the energies $\vec{E}^2$ and $\vec{E}^3$ which compensate the insufficiency of $\vec{E}^1$. Using the energy minimization approach, we obtain that the energies magnitudes are minimized when M_1 and M_2 are respectively associated with targets T_1 and T_2 (see Table 3).

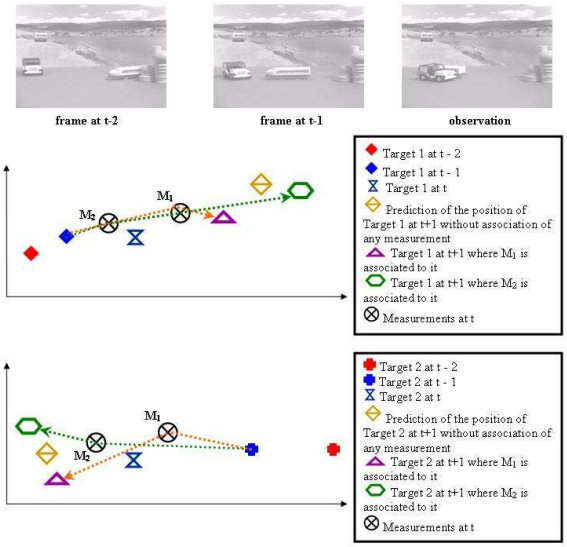

Figure 4: Van Plane test. In the first row: left and middle images represent the frames at $\{t-2, t-1\}$ where two targets $\{T_1, T_2\}$ are present; right image is the real frame at t. The available observation at t contains two measurements $\{M_1, M_2\}$. In the second and third rows, we show the position of both targets at different instants.

Table 3: Energy magnitude computation for both targets when the measurements $\{M_1, M_2\}$ are associated with them.

k	$\alpha_i \|(\vec{E}_k^i)_{M_1}\|$			$\|(\vec{E}_k)_{M_1}\|$
1	0.3141	0.02	0.3429	0.2687
2	0.6858	0.98	0.6571	0.7879
k	$\alpha_i \|(\vec{E}_k^i)_{M_2}\|$			$\|(\vec{E}_k)_{M_2}\|$
1	0.3179	0.7236	0.8636	0.6759
2	0.6821	0.2764	0.1364	0.4322

3.3 Walking Men Test

The "Walking men" sequence shows: Figure 5.a three men walking close at intant $(t-2)$, Figure 5.b, at $t-1$, two men (T_2 and T_3) continue walking in the same direction, while the third one (T_1) takes the opposite direction.

The available observation at t contains three measurements corresponding to positions in the target space (x, y). In Figure 5.c, we show the corresponding frame at instant t where we observe a partial occlusion between two walking men. We have put the measurements in Table 4 in a way that the measurement M_i is generated by the target T_i. We notice that the observed positions of the cross men are very close. Figure 5.d represents the real frame at instant $t+1$ where we remark that the cross men change their directions. We remark from Table 4 that the measurement M_2 is equidistant from targets T_2 and T_3 ($\alpha_2\|(\vec{E}_2^2)_{M_2}\| = \alpha_2\|(\vec{E}_3^2)_{M_2}\| = 0.15$). We also remark from Table 4 that most of time the third energy is null, this effect is due to the presence of a linear movement (motion limited to a displacement in two directions x and y). Once the energies are computed, we obtain the energy magnitude $\|(\vec{E}_i)\|$ is minimized when measurement M_i is associated to target T_i, see the column

Figure 5: Walking men test. (a) Frame at $(t-2)$: three walking men close one to the other; (b) Frame at $t-1$: two men continue walking in the same direction and the third one takes the opposite direction; (c) The observation at t: two men cross and we have a partial occlusion between them; (d) Frame at $t+1$: the cross men change their directions.

Table 4: Energy magnitude computation for targets k when measurements M_i are associated with them.

k	$\alpha_i \|(\vec{E}_k^i)_{M_1}\|$			$\|(\vec{E}_k)_{M_1}\|$
1	0.144	0.03	0	**0.085**
2	0.411	0.82	0	0.53
3	0.444	0.16	0	0.47
k	$\alpha_i \|(\vec{E}_k^i)_{M_2}\|$			$\|(\vec{E}_k)_{M_2}\|$
1	0.70	0.16	0.5	0.51
2	0.15	0.22	0.5	**0.32**
3	0.15	0.62	0	0.37
k	$\alpha_i \|(\vec{E}_k^i)_{M_3}\|$			$\|(\vec{E}_k)_{M_3}\|$
1	0.63	0.0037	0	0.363
2	0.21	0.76	0	0.455
3	0.16	0.235	0	**0.16**

of $\|(\vec{E}_k)_{M_i}\|$ in Table 4. Despite the change in illumination, the measurements were correctly associated to targets by using the approach of energy minimization.

3.4 Window Men Test

In this sequence we observe, at instant $t-2$, two targets: the first one is static and the second undergoes a linear movement (see Figure 6.a). At instant $t-1$, only the second target continues walking and goes near to the first one, Figure 6.b. At instant t, an observation containing two measurements, containing positions, is available. Notice that the observed positions are close and there is a partial occlusion between both targets. Table 5 shows that the distance from measurement M_2 to target T_1 is less than the distance from M_2 to T_2, $\|(\vec{E}_1^1)_{M_2}\| < \|(\vec{E}_2^1)_{M_2}\|$, which leads to a contradiction with the reality. We compute the second energy to compensate the first one. The third energy is null due to the linear displacement of both targets. As we can remark from Table 5, the energy magnitude $\|(\vec{E}_k)_{M_1}\|$ and $\|(\vec{E}_k)_{M_2}\|$ are minimized when M_1 and M_2 are associated with T_1 and T_2 respectively. We remark that our approach of energy minimization gives a correct association despite the presence of a light reflexion on the window.

Figure 6: Window men test. (a) Frame at $t-2$: two targets are present; (b) Frame at $t-1$: both targets are close; (c) the available observation at t; (d) Frame at intant t: both targets move.

Table 5: Energy magnitude computation for targets k when measurements M_i are associated with them.

k	$\|(\vec{E}_k^i)_{M_1}\|$			$\alpha_i\|(\vec{E}_k^i)_{M_1}\|$			$\|(\vec{E}_k)_{M_1}\|$
1	0	0	0	0	0	0	0
2	0.0607	6.2	0	1	1	0	0.82
k	$\|(\vec{E}_k^i)_{M_2}\|$			$\alpha_i\|(\vec{E}_k^i)_{M_2}\|$			$\|(\vec{E}_k)_{M_2}\|$
1	0.0217	0.36	0	0.3	0.83	0	0.51
2	0.0518	0.07	0	0.7	0.16	0	0.42

3.5 Ant Sequence Test

We have tested our method on another sequence showing ants having complex motions. They move with a non-constant velocity and can accelerate, decelerate and sometimes stop moving or starting. These ants are quite similar even non-distinguishable and characterized by the same gray level distribution. The sensor, at instant t, provides an observation containing six measurements corresponding to positions in the (x,y) space. In such scene, only one information can be used: the motion. We remark from Figure 7 that their displacement is erratic. The ants change their direction, accelerate, decelerate, stop moving, do rotation around their axis, *etc*. Figure 7.(a-b) are the acquisitions at instant $t-2$ and $t-1$ and represents the frames 10 and 25 of the ant sequence. We remark there is a considerable interval of time between these two frames. We have labeled the ants just to show their displacements from one frame to another. Figure 7.c shows the available observation at t and represents the frame 35 of the sequence. Figure 7.d is the real frame at $t+1$. Table 6 contains the numerical values of all energies computed between measurements and targets. We have multiplied each one by 100 to show clearly the difference between them. We have also fixed the order of classification in Table 6 so that the measurement M_i is provided from target T_i. If we use the Nearest Neighbor filter to associate the available observations, the measurements $\{M_2, M_4, M_5\}$ will be respectively associated with targets $\{T_4, T_2, T_2\}$ which leads to a contradiction with the reality (see the energy $\alpha_1\|(\vec{E}_k^1)_{M_i}\|$ in Table 6). To remedy, we associate our observations by using the energy minimization approach. We remark from Table 6 that the energies $\alpha_2\|(\vec{E}_2^2)_{M_2}\| < \alpha_2\|(\vec{E}_4^2)_{M_2}\|$ and $\alpha_3\|(\vec{E}_2^3)_{M_2}\| < \alpha_3\|(\vec{E}_4^3)_{M_2}\|$ which compensates the error given by $\alpha_1\|(\vec{E}_2^1)_{M_2}\|$. Finally, the following result is obtained: $\|(\vec{E}_k)_{M_2}\|$ is minimized when M_2 is associated with target T_2. We recite that a measurement is associated with a target if the magnitude of its energy is minimal (equation 5). Lets take another example to show the necessity of using the energy $\vec{E}^3$ in our formulation to compensate the others one. If we only use the energies $\alpha_1\|(\vec{E}_k^1)_{M_i}\|$ and $\alpha_2\|(\vec{E}_k^2)_{M_i}\|$ to associate data, we will get the following result: $\|(\vec{E}_6)_{M_5}\| < \|(\vec{E}_5)_{M_5}\|$ and the measurement M_5 will be associated with target T_6 which leads to an error in association. We can remark from Table 6 that $\alpha_3\|(\vec{E}_5^3)_{M_5}\| < \alpha_3\|(\vec{E}_6^3)_{M_5}\|$ which compensate the other energies. Finally, we observe that each measurement is well associated with its corresponding target. We notice that our approach is not time-consumer. The total time of computation of all these energies is 0.25 seconds. We have used Matlab to implement our method.

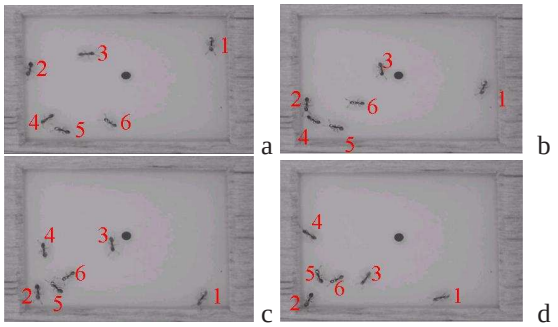

Figure 7: Ant sequence. Frames $\{10, 25, 35, 45\}$. (a-b) Acquisitions at $t-2$ and $t-1$; (c) Available observation at t; (d) Frame at $t+1$.

4 CONCLUSION

This work proposes a new method for data association based on an energy minimization. The developed approach can handle complex motions and highly non-linear systems, and deals with the lack of prior knowledge. Its effectiveness returns to the fact it requires few parameters. The geometric illustration of energy components allows to measure the accuracy between two dynamic models and to define their degree of similarity. As a perspective, we suggest to integrate the energy minimization approach within the classical particle filter to build a new framework for multiple tracking objects. Moreover, since we consider erratic motions that cannot be learned from training sequences, we suggest to use an adaptive and automated way to set the parameters of the dynamic model of the filter. The purpose of developing this framework is to track targets under the restriction of the missing of prior information and especially when similar targets are evolving in the scene. This phase is currently under development.

REFERENCES

Abed, A. E., Dubuisson, S., and Béréziat, D. (2006). Comparison of statistical and shape-based approaches for non-rigid motion tracking with missing data using a particle filter. In *Advanced Concepts for Intelligent Vision Systems*.

Blake, A. and Isard, M. (1998). Active contours. In *Springer-Verlag*.

Fortmann, T., Bar-Shalom, Y., and Scheffe, M. (1983). Sonar tracking of multiple targets using joint probabilistic data association. In *IEEE Journ. Oceanic Engineering*.

North, B., Blake, A., Isard, M., and Rittscher, J. (2000). Learning and classification of complex dynamics. In *IEEE Transactions on Pattern Analysis and Machine Intelligence*.

Rasmussen, C. and Hager, G. (2001). Probabilistic data association methods for tracking complex visual objects. In *IEEE Transactions on Pattern Analysis and Machine Intelligence*.

Rong, L. and Bar-Shalom, Y. (1996). Tracking in clutter with nearest neighbor filter: analysis and performance. In *IEEE transactions on aerospace and electronic systems*.

Vermaak, J., Godsill, S., and Pérez, P. (2005). Monte carlo filtering for multi-target tracking and data association. In *IEEE Transactions on Aerospace and Electronic Systems*.

Table 6: First column and first row contain ant's numbers and measurement's numbers. The energies magnitude are multiplied by 100.

	$\alpha_1 \|\|(\vec{E}_k^1)_{M_i}\|\| \times 100$					
	1	2	3	4	5	6
1	6.512	47.239	25.761	43.975	48.705	46.618
2	22.545	5.762	21.381	**6.498**	**2.510**	12.014
3	15.105	24.891	**4.043**	17.747	23.748	19.693
4	21.447	**1.728**	21.604	9.403	5.444	10.209
5	18.317	6.094	17.943	12.191	**9.276**	5.953
6	16.074	13.549	9.268	10.923	**10.318**	5.513

	$\alpha_2 \|\|(\vec{E}_k^2)_{M_i}\|\| \times 100$					
	1	2	3	4	5	6
1	1.487	1.848	1.424	1.081	11.276	1.091
2	3.096	1.234	3.091	9.610	54.460	1.583
3	14.168	0.234	0.343	0.160	1.256	0.107
4	6.564	2.211	2.669	0.307	24.120	4.400
5	74.366	85.842	92.240	96.185	**6.993**	92.438
6	0.320	0.255	0.233	1.032	**1.895**	0.381

	$\alpha_3 \|\|(\vec{E}_k^3)_{M_i}\|\| \times 100$					
	1	2	3	4	5	6
1	0.037	45.813	0.792	14.091	48.144	43.240
2	6.801	0.014	24.593	0.225	14.570	13.635
3	22.205	8.488	1.783	5.637	4.657	24.499
4	38.757	14.837	27.829	0.708	17.822	12.073
5	8.457	10.537	12.624	3.231	**4.048**	6.203
6	23.743	20.101	32.380	76.319	**10.759**	0.350

	$\|\|(\vec{E}_k)_{M_i}\|\| \times 100$					
	1	2	3	4	5	6
1	**3.856**	38.008	14.903	26.668	40.071	36.715
2	13.713	**3.402**	18.899	6.699	32.580	10.532
3	17.530	15.184	**2.559**	10.751	13.991	18.148
4	25.853	8.718	20.399	**5.447**	17.598	9.475
5	44.487	50.057	54.741	56.008	**7.103**	53.600
6	16.555	13.996	19.446	44.516	8.676	**3.197**